

Radiation enhancement due to metamaterial substrates from an inverse source theory

Mohamed R. Khodja and Edwin A. Marengo

Department of Electrical and Computer Engineering, Northeastern University, Boston, Massachusetts 02115, USA

(Received 29 October 2007; published 14 April 2008)

In this paper the formalism of the electromagnetic inverse source theory is used to investigate radiation enhancement due to antenna substrates. Particular attention is given to sources that are confined within a spherical volume and are embedded within two nested spheres of arbitrary materials. Emphasis is given to the special case when the two nested spheres are made up of materials with oppositely signed constitutive parameters. The analysis comprises forward, or radiation, characterization for a given configuration as well as inverse-theoretic characterization. The forward characterization is focused on the singular-value spectrum of the linear source-to-field mapping relevant to each configuration while the inverse-theoretic characterization is performed via the so-called “minimum-energy” sources capable of generating a prescribed exterior field. The derived formulation is based on constrained optimization and multipole theory. Importantly, it is non-antenna-specific. Thus, this formulation enables fair comparison of different substrate configurations by comparing optimal radiation in each configuration (i.e., the “best” in each one), as governed by a formally tractable source-energy cost function that is physically motivated by Ohmic loss control. The derived theory is accompanied by numerical results illustrating the effects on radiation enhancement of particular substrate designs.

DOI: [10.1103/PhysRevE.77.046605](https://doi.org/10.1103/PhysRevE.77.046605)

PACS number(s): 41.20.-q, 84.40.Ba, 02.30.Zz

I. INTRODUCTION

The study of materials exhibiting anomalous responses to different types of excitation has a long history that dates back at least to the late part of the nineteenth century [1–3]. However, it was not until the experimental realization, in 2000, of a particular type of what are now widely known as metamaterials, namely, a composite medium exhibiting a negative index of refraction in the microwave regime [4], that these electromagnetically engineered materials really caught the attention of the scientific and engineering communities.

The utilization of antenna-embedding substrates (and metamaterials, in particular) to enhance the performance of an antenna has been investigated by several groups [5–31]. (An expanded bibliography can be found in Ref. [32].) Motivated by the identified possibility of embedding an antenna in a metamaterial substrate so as to generate a certain field or performance level that may be unachievable, under comparable physical constraints, i.e., resources, including antenna size, if radiating in the vacuum, we present in this paper a non-antenna-specific analysis of radiation and source inversion in substrate media that is a generalization of the scalar inverse source theory in background media in Ref. [33] and a continuation and extension of our recent full-vector analysis in Refs. [34,35]. Unlike Refs. [33–35], where the focus is homogeneous substrates, the present study goes a step further by addressing an important layered medium that has been at the heart of key investigations in the field of antenna substrate enhancement.

In particular, to present our general non-antenna-specific theory of substrate enhancement in a context that relates to important work by other groups in this area, particular emphasis is given in the following to embedding media formed by two nested spheres of different materials. This particular configuration is of great practical importance for both antenna radiation and scattering and hence imaging resolution enhancement. It enables enhancements that are more dra-

matic than those due to homogeneous substrates. The radiative as well as the scattering properties of a system of two nested spheres of ordinary materials associated with a dipole have been considered by several authors [36–39]. These studies have now been extended to cases where metamaterials are present. For instance, Gao and Huang [40] have calculated the extinction efficiency of the core-shell system. Following the steps of Aden and Kerker [41], Alù and Engheeta [42,43] have looked at the resonant scattering that arises when the two spheres are constructed by combining a pair of materials with oppositely signed constitutive parameters. Ziolkowski and Kipple [15] have established the reciprocity of the peculiar scattering properties described by Alù and Engheeta [42] and the enhanced radiation power they realized would occur when an electrically small dipole antenna is surrounded by a metamaterial shell [9].

The geometry of the system to be investigated in the following is that of two nested spheres immersed in the vacuum (refer to Fig. 1). The inner sphere, of radius a , has relative electric permittivity $\epsilon_a \equiv \epsilon_{\text{sphere}}/\epsilon_0$ and relative magnetic per-

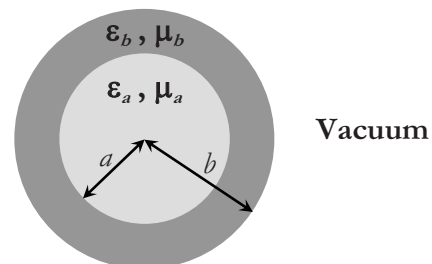


FIG. 1. Geometry of the three-region system under consideration. The driving points and material structure of the antenna are confined within a spherical volume V of radius a . The inner sphere of radius a has relative permittivity ϵ_a and relative permeability μ_a . This inner sphere is surrounded by a spherical shell of inner radius a and outer radius b and has relative permittivity ϵ_b and relative permeability μ_b . The core-shell system is immersed in the vacuum.

meability $\mu_a \equiv \mu_{\text{sphere}}/\mu_0$. This inner sphere constitutes the core of the system and is the smallest spherical volume V that circumscribes the largest physical dimension of the original antenna which is treated next, under a suppressed time dependence $e^{-i\omega t}$, as a primary, or impressed, current density $\mathbf{J}(\mathbf{r})$. The core is surrounded by a spherical shell, of inner radius a and outer radius b . The relative constitutive parameters of the shell are relative electric permittivity $\epsilon_b \equiv \epsilon_{\text{shell}}/\epsilon_0$ and relative magnetic permeability $\mu_b \equiv \mu_{\text{shell}}/\mu_0$. Thus the resulting three-region system may be characterized by a total electric permittivity distribution of the form

$$\frac{\epsilon(\mathbf{r})}{\epsilon_0} = \epsilon_a \Theta(a-r) + \epsilon_b [\Theta(r-a)\Theta(b-r)] + \Theta(r-b) \quad (1)$$

and a total magnetic permeability distribution of the form

$$\frac{\mu(\mathbf{r})}{\mu_0} = \mu_a \Theta(a-r) + \mu_b [\Theta(r-a)\Theta(b-r)] + \Theta(r-b), \quad (2)$$

where Θ denotes Heaviside's unit step function [$\Theta(x)=1$, for $x \geq 1$, otherwise $\Theta(x)=0$], and ϵ_0 and μ_0 are, respectively, the electric permittivity and magnetic permeability of the vacuum.

The core and the surrounding shell, being assumed to be generally lossy, are assigned relative constitutive parameters that are complex. These constitutive parameters are, thus, assumed to have the generic forms $\epsilon_\alpha = \text{Re}[\epsilon_\alpha] + i \text{Im}[\epsilon_\alpha]$ and $\mu_\alpha = \text{Re}[\mu_\alpha] + i \text{Im}[\mu_\alpha]$, $\alpha = a, b$ (where a is for the inner sphere and b is for the outer shell.) Note that the losses are indicated by the presence of non-negative imaginary parts of the permittivity and the permeability. (The non-negativity of $\text{Im}[\epsilon_\alpha]$ and $\text{Im}[\mu_\alpha]$ is necessary for passive materials.) There exist different terminologies to describe the different types of metamaterials, here we adopt the following one: when $\text{Re}[\epsilon_\alpha] > 0$ and $\text{Re}[\mu_\alpha] > 0$ the material is said to be double positive (DPS); when $\text{Re}[\epsilon_\alpha] < 0$ and $\text{Re}[\mu_\alpha] < 0$ the material is said to be double negative (DNG); and when $\text{Re}[\epsilon_\alpha]\text{Re}[\mu_\alpha] < 0$ the material is said to be single negative (SNG). (A more detailed terminology labels materials for which $\text{Re}[\epsilon_\alpha] < 0$ as ENG or ϵ -negative media, and materials for which $\text{Re}[\mu_\alpha] < 0$ as MNG or μ -negative media.) These particular choices for the signs of the constitutive parameters are required if wave propagation in the medium is to be causal [44].

The approach adopted next is to formulate an inverse source problem in substrate media, whose objective is to deduce an unknown primary current density $\mathbf{J}(\mathbf{r})$ that is contained, along with the substrate, in the spherical volume V , and that generates a prescribed exterior field for $|\mathbf{r}| > b$. Theoretically, there can be nonradiating source components [45,46] within the source region. Consequently, if $\mathbf{J}(\mathbf{r})$ is a solution to the inverse source problem then one can add any nonradiating source to generate another valid solution whose generated field for $|\mathbf{r}| > b$ coincides with the desired exterior field. Thus one must impose additional constraints to guarantee the uniqueness of the solution. The most commonly adopted constraint is that of minimizing the square of the L^2 norm of the source [as defined in Eq. (6)], usually termed

“the source energy” in the inverse problems literature. It is at the heart of the Picard conditions defining the range of the source-to-field linear mapping from L^2 sources to L^2 far fields. It has also been used, recently, in addressing the realizability of electromagnetic pulsed beams or wavelet fields launchable from finite-size sources [47,48]. The solution to the inverse source problem that minimizes the source energy is usually termed “the minimum (source) energy solution.” It is related to the real image field generated by a point-reference hologram of the field recorded on a closed surface completely surrounding the source volume [49–51]. The ability of an antenna to radiate a prescribed field with reduced current levels as characterized by this norm is an indication of efficiency which has been used as constraint in antenna synthesis [52–56]. Reduction of the source energy also accounts for reduction of Ohmic losses in driving metallic elements, thus this constraint is of both mathematical convenience as well as physical importance.

A minimized source energy would indicate that the resources of the antenna generating the given field pattern are optimally used within the prescribed volume of the source. Furthermore, comparison of the required minimum source energies for different substrate configurations enables quantification of the enhancement due to such structures. Upon solving the inverse source problem in these media for the prescribed exterior fields, one can proceed to tackle the comparison of the required resources, embodied in the source functional energy in the present case, that are needed for the launching of the given fields. Substrate configurations for which the required source energy is lower are then more optimal than alternative configurations which require higher source energy for the launching of the same fields. This mathematical framework to characterize substrate enhancement is non-device-specific, in particular, one is then comparing the “best” source, which minimizes the required source energy for the launching of the given field via a given substrate, versus the “best” source, which minimizes the source energy for the launching of the same field but at a different substrate (including the “no-substrate” or free space case).

It is important to point out that the present formulation of the inverse source problem in the two-nested-spheres configuration is also relevant to that of the companion inverse scattering problem. In fact, it is mathematically equivalent to that of an inverse scattering problem in which a single incident field is used as excitation. Hence, the results on the inverse source problem and on the possibility of extracting higher spatial frequency information about the unknown object thanks to the presence of the embedding medium [33] also point out the possibility of similarly enhancing imaging resolution in the associated inverse scattering problem with helper substrate media. In addressing the inverse source problem in these media one is automatically paving the way for inverse scattering formulations in such media. This is particularly pertinent in the modern context of so-called qualitative imaging methods based on support estimation of induced sources and which are noniterative (e.g., linear sampling, factorization method, time-reversal MUSIC, and so on) [57–59]. Those inverse scattering methods are of the

so-called ‘‘inverse-source’’ type, in other words, they are based on a companion inverse source problem.

II. THE RADIATION PROBLEM

The vector wave equation which governs the behavior of the electric field $\mathbf{E}(\mathbf{r})$ produced by a primary current density $\mathbf{J}(\mathbf{r})$ (i.e., the source) confined within the spherical volume V (of radius a , and centered about the origin) is

$$\nabla \times \left(\frac{\nabla \times \mathbf{E}(\mathbf{r})}{\mu(\mathbf{r})} \right) - \omega^2 \epsilon(\mathbf{r}) \mathbf{E}(\mathbf{r}) = i\omega \mathbf{J}(\mathbf{r}). \quad (3)$$

The outgoing-wave dyadic Green function $\bar{\mathbf{G}}(\mathbf{r}, \mathbf{r}')$ associated with the partial differential operator in Eq. (3) satisfies, along with the radiation condition [60], the differential equation

$$\nabla \times \left(\frac{\nabla \times \bar{\mathbf{G}}(\mathbf{r}, \mathbf{r}')}{\mu(\mathbf{r})} \right) - \omega^2 \epsilon(\mathbf{r}) \bar{\mathbf{G}}(\mathbf{r}, \mathbf{r}') = i\omega \delta(\mathbf{r} - \mathbf{r}') \bar{\mathbf{I}}, \quad (4)$$

where $\bar{\mathbf{I}}$ denotes the identity dyadic and δ the Dirac delta. In terms of $\bar{\mathbf{G}}(\mathbf{r}, \mathbf{r}')$ the solution of Eq. (3) can be cast in the form

$$\mathbf{E}(\mathbf{r}) = \int_V d\mathbf{r}' \bar{\mathbf{G}}(\mathbf{r}, \mathbf{r}') \cdot \mathbf{J}(\mathbf{r}'). \quad (5)$$

It is convenient to define the inner product $(\mathbf{f}, \mathbf{f}') = \int_V d\mathbf{r} \cdot \mathbf{f}^*(\mathbf{r}) \cdot \mathbf{f}'(\mathbf{r})$ where the asterisk $*$ denotes the complex conjugate, and \mathbf{f} and \mathbf{f}' are any two functions of position. In this notation, the square of the L^2 norm of the source, also called ‘‘source energy,’’ is given by

$$\mathcal{E} \equiv (\mathbf{J}, \mathbf{J}). \quad (6)$$

On the other hand, the complex interaction power \mathcal{P} (see, for instance, Refs. [61,62]) is

$$\mathcal{P} = -\frac{1}{2} (\mathbf{J}, \mathbf{E}). \quad (7)$$

To formulate the inverse problem for the cases described in Eqs. (1) and (2) it is necessary to first solve the associated radiation problem. To accomplish this, we note that in the exterior region corresponding to $|\mathbf{r}| > b$ the electric field $\mathbf{E}(\mathbf{r})$ can be represented by the multipole expansion [61,63]

$$\mathbf{E}(\mathbf{r}) = \sum_{j=1}^2 \sum_{l=1}^{\infty} \sum_{m=-l}^l a_{l,m}^{(j)} \mathbf{\Lambda}_{l,m}^{(j)}(\mathbf{r}), \quad (8)$$

where the complex-valued expansion coefficients $a_{l,m}^{(j)}$ are the multipole moments of the field, and where $\mathbf{\Lambda}_{l,m}^{(j)}$ are the multipole fields given by

$$\mathbf{\Lambda}_{l,m}^{(j)}(\mathbf{r}) \equiv \begin{cases} \nabla \times [h_l^{(+)}(k_0 r) \mathbf{Y}_{l,m}(\hat{\mathbf{r}})], & j=1, \\ ik_0 h_l^{(+)}(k_0 r) \mathbf{Y}_{l,m}(\hat{\mathbf{r}}), & j=2, \end{cases} \quad (9)$$

where $\hat{\mathbf{r}} \equiv \mathbf{r}/r$, $h_l^{(+)}$ denotes the spherical Hankel function of the first kind and order l (as defined in Ref. [64]), corresponding to outgoing spherical waves, $\mathbf{Y}_{l,m}$ is the vector spherical harmonic of degree l and order m (as defined in Ref. [63]), and $j=1$ and $j=2$ correspond to electric and magnetic multipole fields, respectively. Physically, the index l characterizes the multipolarity (or modal order) of the field; thus $l=1$ corresponds to 2¹-pole (dipole) radiation, $l=2$ corresponds to 2²-pole (quadrupole) radiation, $l=3$ corresponds to 2³-pole (octupole) radiation, and so on. Note that in Eq. (8) the summation over l starts from $l=1$ because there are no vector spherical harmonics of zero degree [63].

The electric and magnetic multipole moments, $a_{l,m}^{(1)}$ and $a_{l,m}^{(2)}$, respectively, are related to the current distribution \mathbf{J} by

$$a_{l,m}^{(j)} = (\mathfrak{B}_{l,m}^{(j)}, \mathbf{J}), \quad j=1,2, \quad (10)$$

i.e., they are the projections of the current distribution \mathbf{J} onto the set of source-free vector fields $\mathfrak{B}_{l,m}^{(j)}$ which need to be determined for the particular antenna background medium. These fields are closely related to the familiar source-free multipole fields that appear in the free-space case [63,65]. It is shown in the Appendix that for backgrounds whose permittivity and permeability are given by Eqs. (1) and (2) one has

$$\mathfrak{B}_{l,m}^{(j)} \equiv \begin{cases} \frac{-\eta_0}{l(l+1)} \mathfrak{F}_l^{*(1)} \nabla \times [j_l(k_a^* r) \mathbf{Y}_{l,m}(\hat{\mathbf{r}})], & j=1, \\ \frac{-ik_0 \eta_0}{l(l+1)} \mathfrak{F}_l^{*(2)} j_l(k_a^* r) \mathbf{Y}_{l,m}(\hat{\mathbf{r}}), & j=2, \end{cases} \quad (11)$$

where j_l is the spherical Bessel function of the first kind and order l (as defined in Ref. [64]), and $k_a = \omega \sqrt{\epsilon_a \epsilon_0 \mu_a \mu_0}$ is the inner sphere substrate wave number and where we have defined

$$\mathfrak{F}_l^{(j)} \equiv \begin{cases} \frac{-\epsilon_b}{\Delta_1 k_0 k_b a^2 b^2}, & j=1, \\ \frac{-\mu_a \mu_b}{\Delta_2 k_0 k_b a^2 b^2}, & j=2, \end{cases} \quad (12)$$

where [cf. Equations (26),(27) in Ref. [41] and Eqs. (8),(9) in Refs. [42,43]]

$$\Delta_1 = \begin{vmatrix} 0 & k_b U_l(k_b b) & k_b V_l(k_b b) & -k_0 V_l(k_0 b) \\ 0 & \epsilon_b j_l(k_b b) & \epsilon_b h_l^{(+)}(k_b b) & -h_l^{(+)}(k_0 b) \\ k_a U_l(k_a a) & -k_b U_l(k_b a) & -k_b V_l(k_b a) & 0 \\ \epsilon_a j_l(k_a a) & -\epsilon_b j_l(k_b a) & -\epsilon_b h_l^{(+)}(k_b a) & 0 \end{vmatrix} \quad (13)$$

and

$$\Delta_2 = \begin{vmatrix} 0 & j_l(k_b b) & h_l^{(+)}(k_b b) & -h_l^{(+)}(k_0 b) \\ 0 & \frac{k_b}{\mu_b} U_l(k_b b) & \frac{k_b}{\mu_b} V_l(k_b b) & -k_0 V_l(k_0 b) \\ j_l(k_a a) & -j_l(k_b a) & -h_l^{(+)}(k_b a) & 0 \\ \frac{k_a}{\mu_a} U_l(k_a a) & -\frac{k_b}{\mu_b} U_l(k_b a) & -\frac{k_b}{\mu_b} V_l(k_b a) & 0 \end{vmatrix}. \quad (14)$$

In Eqs. (13) and (14) the quantities U_l and V_l are defined such that

$$U_l(kr) \equiv \frac{dj_l(kr)}{d(kr)} + \frac{j_l(kr)}{kr} \quad (15)$$

and

$$V_l(kr) \equiv \frac{dh_l^{(+)}(kr)}{d(kr)} + \frac{h_l^{(+)}(kr)}{kr}. \quad (16)$$

Note that in Eqs. (12)–(14) $k_0 = \omega\sqrt{\epsilon_0\mu_0}$ and $k_b = \omega\sqrt{\epsilon_b\epsilon_0\mu_b\mu_0}$ are the propagation constants in the vacuum and in the shell, respectively. Also, it is clear from Eqs. (12)–(16) that the parameters $\mathfrak{F}_l^{(j)}$ are not constants but in fact functions of several parameters.

It is not hard to show that the terms $\mathfrak{F}_l^{(j)}$ reduce to the Mie amplitudes $F_l^{(j)}$, as defined in Refs. [33–35], when $a=b$, as expected. Consequently, they also reduce to unity in the free-space case, i.e., when $a=b$, $\epsilon_a=1=\epsilon_b$, and $\mu_a=1=\mu_b$, causing Eqs. (11) to reduce to the free-space case equations [65,66]. Substitution of the associated results into Eq. (10) completes the description of the forward problem. Armed with these developments, we are in position to formulate next the corresponding inverse source problem.

III. INVERSE SOURCE THEORY BASED ON CONSTRAINED OPTIMIZATION

The inverse source problem of deducing the source $\mathbf{J}(\mathbf{r})$, confined within V and embedded in a given background medium obeying Eqs. (1) and (2), from knowledge of the exterior field $\mathbf{E}(\mathbf{r})$ for $|\mathbf{r}|>b$, or according to the discussion in Eqs. (A13)–(A16), the far-field radiation pattern, is seen from Eqs. (8), (9), and (A13)–(A16) to be equivalent to that of determining the source from knowledge of the multipole moments, i.e., to that of inverting Eqs. (10). The respective inversion is addressed next via a generalization of the free-space optimization theory in Ref. [67] to nonhomogeneous backgrounds along lines analogous to those in Refs. [33,34]. Emphasis is given to the particular case of piecewise-constant radially symmetric backgrounds, but the derived expressions apply to more general cases as long as one uses the appropriate projective wave functions $\mathfrak{B}_{l,m}^{(j)}$ which vary from a medium type to another.

The problem of determining the minimum-energy source of support V generating a given exterior field (for $|\mathbf{r}|>b$) can be mathematically cast into an optimization problem whose

solution reduces to the determination of the complex-valued Lagrange multipliers $C_{l,m}^{(j)}$ that extremize the generalized Lagrangian

$$\mathcal{L} = \mathcal{E} + 2 \operatorname{Re} \left[\sum_{j=1}^2 \sum_{l=1}^{\infty} \sum_{m=-l}^l C_{l,m}^{(j)} \{a_{l,m}^{(j)} - (\mathfrak{B}_{l,m}^{(j)} \mathbf{J})\} \right], \quad (17)$$

where the source energy \mathcal{E} is defined by Eq. (6). By requiring that the first variation of the Lagrangian vanish, one finds that the minimum-energy source is given by

$$\mathbf{J}_{\text{ME}} = \sum_{j=1}^2 \sum_{l=1}^{\infty} \sum_{m=-l}^l \frac{a_{l,m}^{(j)}}{[\sigma_l^{(j)}]^2} \mathfrak{B}_{l,m}^{(j)} \quad (18)$$

and that the corresponding minimum source energy is

$$\mathcal{E}_{\text{ME}} = \sum_{j=1}^2 \sum_{l=1}^{\infty} \sum_{m=-l}^l \frac{|a_{l,m}^{(j)}|^2}{[\sigma_l^{(j)}]^2}, \quad (19)$$

where we have introduced the positive-definite singular values

$$[\sigma_l^{(j)}]^2 \equiv (\mathfrak{B}_{l,m}^{(j)}, \mathfrak{B}_{l,m}^{(j)}) \equiv |\mathfrak{F}_l^{(j)}|^2 [\kappa_l^{(j)}]^2, \quad (20)$$

where

$$[\kappa_l^{(j)}]^2 \equiv \begin{cases} \eta_0^2 \int_0^a dr \left[|j_l(k_a r)|^2 + \frac{|k_a r|^2}{l(l+1)} |U_l(k_a r)|^2 \right], & j=1, \\ \frac{\eta_0^2 k_0^2}{l(l+1)} \int_0^a dr r^2 |j_l(k_a r)|^2, & j=2. \end{cases} \quad (21)$$

In Refs. [34,35] analytical expressions were derived for the integrals appearing in Eq. (21), for $k_a^2 \in \mathbb{R}$, by means of Lommel's second integral. In the general case, however, the complex argument of the Bessel functions makes it necessary to recur to numerical methods of integration.

We define the dimensionless positive-definite normalized singular values

$$[\varrho_l^{(j)}]^2 \equiv \frac{[\sigma_l^{(j)}]^2}{[\sigma_l^{(j)}(\text{free-space case})]^2}, \quad (22)$$

where $[\sigma_l^{(j)}(\text{free-space case})]^2$ are the singular values that correspond to the free-space case. Subsequently, $[\varrho_l^{(j)}]^2$ will be referred to, simply, as singular values. The free-space case is defined as the case in which the original antenna, as defined in Sec. I, radiates in the vacuum. Quantitatively this corresponds to the case $a=b$, $\epsilon_a=\epsilon_b=\mu_a=\mu_b=1$. In other words, the reference antenna with respect to which the comparisons are carried out is the original antenna without the shell. This may sound as an unfair comparison, after all the new antenna, i.e., the core-shell system, represents a totally new antenna with its own new dimensions and induced currents due to the addition of the shell to the original antenna. What is more, we allowed, in the numerical simulations, the dimensions of the outer shell to be of comparable size to the core. Consequently, this definition may not sound as the best definition for a reference or standard antenna to measure the enhancement with respect to. Nevertheless, this definition is

underlain by a simple, if not naive, answer to the question of how the addition of a metamaterial shell would affect the performance of an existing antenna, or, similarly, how the embedding of an existing antenna in a given core-shell system with oppositely signed constitutive parameters would affect the performance of the antenna. A more detailed investigation of the effect of reference antennas on enhancement level estimates and the issue of fairness in antenna radiation performance is presented elsewhere [68].

IV. NUMERICAL RESULTS AND CASE STUDIES

In this section we turn to the application of the theory exposed above to the elucidation of the effect of embedding media on antenna radiation performance. The goal is to gain an understanding of the effect of the antenna substrate on the minimum source energy for a given radiation pattern. Because of the dependence of the problem on so many parameters we limit ourselves to a few illustrative cases. Three classes of antennas are investigated: a quarter-wavelength antenna (i.e., $2a=\lambda/4$), a $\lambda/40$ antenna (i.e., $2a=\lambda/40$), and a $\lambda/400$ antenna (i.e., $2a=\lambda/400$). The driving frequency of the antenna is set to $f=3.75$ GHz. This corresponds to $a=1, 0.1, 0.01$ cm, for the $\lambda/4$ antenna, $\lambda/40$ antenna, and $\lambda/400$ antenna, respectively. Needless to say that these particular choices of the numerical values of f and a are arbitrary. However, they lie well within the range of values used in the scientific and engineering literatures [9,15,16,42,43]. Particular attention is paid to electrically small antennas. This is in view of the exciting properties that these antennas exhibit in the subwavelength limit when embedded in a pair of oppositely signed materials. We adopt the definition [69] according to which an electrically small antenna in the vacuum is defined as an antenna for which $k_0a=2\pi a/\lambda \leq 0.5$, where a is the radius of the sphere that encompasses the entire original antenna. Hence, a more detailed investigation is carried out for the $\lambda/400$ multipolar and dipolar antennas. At this point it is appropriate to give one more definition. In the plots and associated discussion we consider the normalized wave number defined by $x_b \equiv k_b/\pi$. The normalized wave number x_b represents the wave number of the field in the shell.

It follows from Eqs. (19) and (22) that, generally, the larger the singular values $[\varrho_l^{(j)}]^2$ the smaller the minimum source energy \mathcal{E}_{ME} required for the launching of a given radiation pattern with a source of a given size. Therefore the larger the singular values $[\varrho_l^{(j)}]^2$ the greater the associated enhancement, due to the associated substrates, of radiation of the l th multipole order field with given resources. It is thus important to understand the dependence of the singular values $[\varrho_l^{(j)}]^2$ on the several parameters it depends on for both the electric ($j=1$) and the magnetic ($j=2$) cases. Large singular values, such as resonances or peaks in the plots of the singular values versus these variables, will indicate enhanced radiation for such operational modes or conditions, with the given resources. This aspect is investigated numerically next. For the sake of conciseness, however, and because of the noted similarity (see next section) between the behavior of the electric singular values and the magnetic singular values

we concentrate our attention in what follows on the study of the electric singular values.

As noted above, there is a tight relationship between the local behavior of the singular values $[\varrho_l^{(j)}]^2$ and the launching ability of the antenna: any resonant peaks in the spectra of $[\varrho_l^{(j)}]^2$ would indicate the presence of local enhancements in the launching ability of the antenna. Nevertheless, it is well known [15,42,43] that the core-shell system does possess a resonant behavior (resonant scattering and resonant radiation) that can be traced back to the presence of the natural modes (polaritons) in the system. Thus we should anticipate the occurrence of such resonant behavior in our case too. The question that arises then is: should they appear, can we ascribe the resonant peaks in the spectra of the singular values $[\varrho_l^{(j)}]^2$ to the presence of polaritons? The conditions for the existence of polaritons in the core-shell system are summarized by their dispersion relations [41–43]

$$\Delta_1 = 0 \quad (23)$$

for the electric modes, where Δ_1 has been defined in Eq. (13), and

$$\Delta_2 = 0 \quad (24)$$

for the magnetic modes, where Δ_2 has been defined in Eq. (14). However, the singular values $[\varrho_l^{(j)}]^2$ are given by Eqs. (20)–(22), i.e., they are composed of two quantities: $|\mathfrak{F}_l^{(j)}|^2$, defined in Eq. (12), and $[\kappa_l^{(j)}]^2$, defined in Eq. (21). It is true that Eqs. (23) and (24) when substituted in the definition of amplitudes $|\mathfrak{F}_l^{(j)}|^2$ [i.e., in Eq. (12)] would provide the resonance conditions (23) and (24) with a very strong effect on the behavior of the singular values $[\varrho_l^{(j)}]^2$. Yet, in order for us to be able to confidently attribute the resonant peaks to the presence of polaritons we have to show that the quantities $[\kappa_l^{(j)}]^2$ do not exhibit a resonant behavior similar to that of $|\mathfrak{F}_l^{(j)}|^2$ that would potentially shift or even kill the peaks created by the resonance conditions of the polaritons. Actually the quantities $[\kappa_l^{(j)}]^2$ are essentially nonpathological combinations of the spherical Bessel functions of the first kind j_l and their derivatives which are sufficiently well-behaved for all integer values of l and complex values of the argument [70]. Hence, we can confidently claim that the spectrum of the singular values $[\varrho_l^{(j)}]^2$ will indeed exhibit resonant peaks, and thus maximum enhancements, and that these peaks will be primarily due to the presence of polaritons as stipulated by the resonance conditions (23) and (24). Finally, we point out that the MATHEMATICA code used for the numerical simulations has been validated against some well-known cases such as the free-space case [67] and the single spherical substrate case (unpublished numerical study in connection with our work in Refs. [34,35]).

A. Lossless substrates

1. Vacuum-core-DPS-shell system

We focus on the case of a spherical shell of non-magnetic lossless DPS material ($\epsilon_b > 1$, $\mu_b = 1$) surrounding an inner sphere with no substrate material in it ($\epsilon_a = 1 = \mu_a$), a system that we will refer to as a vacuum-core-DPS-shell system. In

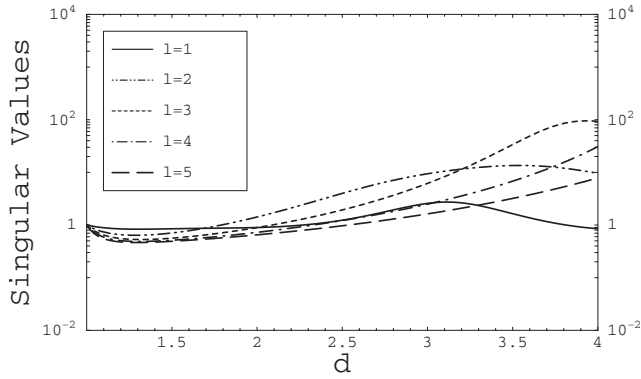


FIG. 2. Logarithmic plot of the normalized electric singular values $[\varrho_l^{(1)}]^2$ for a $\lambda/4$ antenna versus the radii ratio $d \equiv b/a$. The inner sphere is assumed not to contain any material (i.e., $\epsilon_a=1 = \mu_a$) and the surrounding shell is assumed to be a lossless DPS material with $\mu_b=1$ and $x_b=50 \text{ m}^{-1}$.

Figs. 2–4 we plot the electric singular values $[\varrho_l^{(1)}]^2$ versus the radii ratio $d \equiv b/a$, for a quarter-wavelength antenna of maximum length $2a=2 \text{ cm}$ operating at a the frequency $f=3.75 \text{ GHz}$. The plots show that the singular values $[\varrho_l^{(1)}]^2$ exhibit a cyclic behavior with resonant peaks, i.e., local enhancements, appearing at specified values of the radii ratio d . (The same behavior is exhibited by the magnetic singular values $[\varrho_l^{(2)}]^2$, though the plots are not shown here.) As mentioned above these resonant peaks correspond to an enhancement in the launching ability of the antenna for such operational modes with the given resources. The plots also show that for the smaller values of the radii ratio d [by “smaller values” we mean $d \leq r(x_b)$, where $r(x_b)$ is a value that decreases as x_b increases] the best local enhancements, though not always resonant, are observed for the lower multipole modes starting with the dipolar modes. As the radii ratio increases the best enhancements shift to the modes with higher multiplicities: quadrupole, then octupole, and so on. The explanation of this observation is that the higher the multipolarity of the mode the more “intricate” is its structure such that exciting higher multipolarity modes in an efficient way requires thicker shells i.e., shells that possess a “richer”

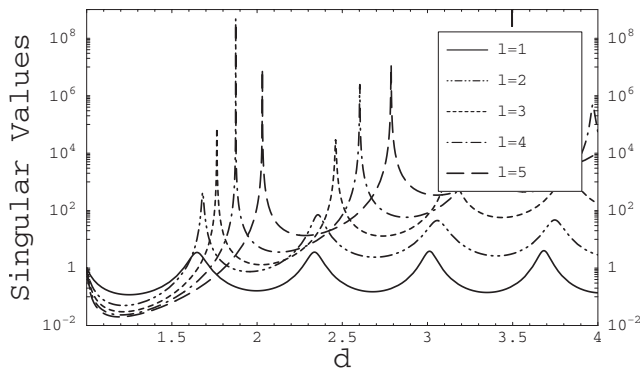


FIG. 3. Logarithmic plot of the normalized electric singular values $[\varrho_l^{(1)}]^2$ for a $\lambda/4$ antenna versus the radii ratio $d \equiv b/a$. The inner sphere is assumed not to contain any material (i.e., $\epsilon_a=1 = \mu_a$) and the surrounding shell is assumed to be a lossless DPS material with $\mu_b=1$ and $x_b=150 \text{ m}^{-1}$.

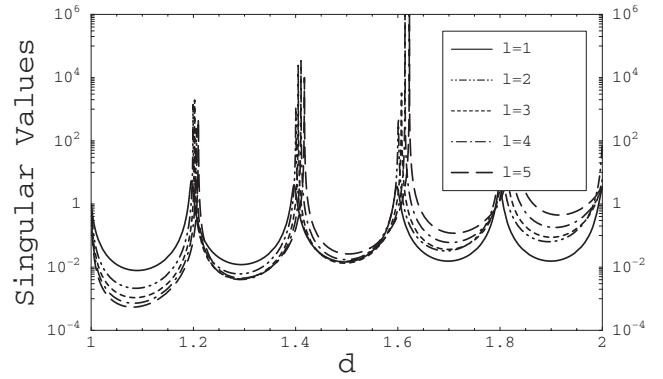


FIG. 4. Logarithmic plot of the normalized electric singular values $[\varrho_l^{(1)}]^2$ for a $\lambda/4$ antenna versus the radii ratio $d \equiv b/a$. The inner sphere is assumed not to contain any material (i.e., $\epsilon_a=1 = \mu_a$) and the surrounding shell is assumed to be a lossless DPS material with $\mu_b=1$ and $x_b=500 \text{ m}^{-1}$.

charge structure. The peaks become sharper and more packed as the electromagnetic density (i.e., the wave number) of the shell material increases. This occurs because as the electromagnetic density of the material increases, i.e., as ϵ_b increases (since $\mu_b=1$, in this case), the ability of a given thickness of the material to support more natural modes of oscillation (i.e., polaritons) also increases. For very electromagnetically dense materials, however, the heights of the peaks saturate indicating a saturation in the launching enhancement levels and the peaks pile up at almost the same values of the radii ratio d , which are now closely packed (see Fig. 4). These closely packed peaks indicate, on the one hand, that an enhancement in the launching ability of the antenna occurs, for high values of the wave number x_b , at almost the same radii ratios for the electromagnetic multipolar modes with a pile up of the resonant peaks at particular values of the radii ratio that is less pronounced for the magnetic modes. On the other hand, this also indicates that the enhancement in the launching ability of the antenna occurs for the two types of fields, i.e., electric and magnetic, at roughly the same values of the radii ratio. Moreover, a closer examination of the plots in Fig. 4 and its magnetic counterpart (figure not shown) reveals that for the electric dipolar mode and its magnetic counterpart, i.e., the magnetic dipolar mode, in particular the local enhancement peaks appear now at almost the same values of the radii ratio $d \approx 1.2, 1.4, 1.6$, etc.

In Fig. 5 we plot the normalized electric singular values $[\varrho_l^{(1)}]^2$ for a $\lambda/400$ antenna versus the radii ratio d . The surrounding shell is assumed to be a lossless nonmagnetic DPS medium with $x_b=150 \text{ m}^{-1}$ (i.e., $\mu_b=1$ and $\epsilon_b=36$). Figure 5 clearly shows that for an electrically small antenna the resonant peaks disappear over the same range of d values that had been considered for a quarter-wavelength antenna and that had in several enhancement peaks present in it in that case. Furthermore, the numerical simulations show that increasing the wave number of the shell medium not only does not restore the peaks but may make things even worse in terms of the launching ability of the antenna with respect to the free-space case. This is in perfect agreement with the fact that the actual total physical dimensions of a resonating cav-

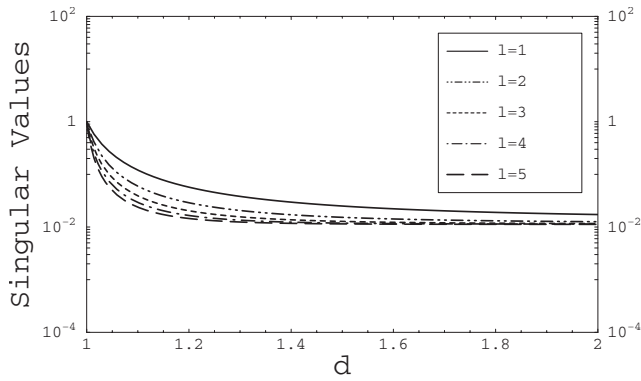


FIG. 5. Logarithmic plot of the normalized singular values $[\rho_l^{(1)}]^2$ for a $\lambda/400$ antenna versus the radii ratio $d \equiv b/a$. The inner sphere is assumed not to contain any material (i.e., $\epsilon_a=1=\mu_a$) and the surrounding shell is assumed to be a lossless DPS material with $\mu_b=1$ and $x_b=150 \text{ m}^{-1}$.

ity made up of ordinary material, in particular $a+b$ in this case, is the determining factor when it comes to which modes are supportable by the cavity, and not just the radii ratio.

2. Vacuum-core-DNG-shell system

The next lossless system we wish to investigate is a vacuum-core-DNG-shell system, i.e., $\epsilon_a=1=\mu_a$, and $\epsilon_b < 0$, $\mu_b < 0$ (in fact in all what follows the relative electric permittivity of the surrounding DNG shells is $\epsilon_b=-4$ and its relative magnetic permeability is $\mu_b=-1$). The driving frequency is as before set to $f=3.75 \text{ GHz}$. In Fig. 6 we plot the electric singular values $[\rho_l^{(1)}]^2$ versus the radii ratio d for a quarter-wavelength antenna of maximum length $2a=2 \text{ cm}$, in Fig. 7 we plot $[\rho_l^{(1)}]^2$ versus d for a $\lambda/40$ antenna of maximum length $2a=0.2 \text{ cm}$, and in Fig. 8 we plot $[\rho_l^{(1)}]^2$ versus d for a $\lambda/400$ antenna of maximum length $2a=0.02 \text{ cm}$. The simulations show that (see Figs. 6–8) as the ratio of the length of the antenna to the wavelength of the radiation in the vacuum, viz., $2a/\lambda$, decreases the resonant peaks, which correspond to a local enhancement in

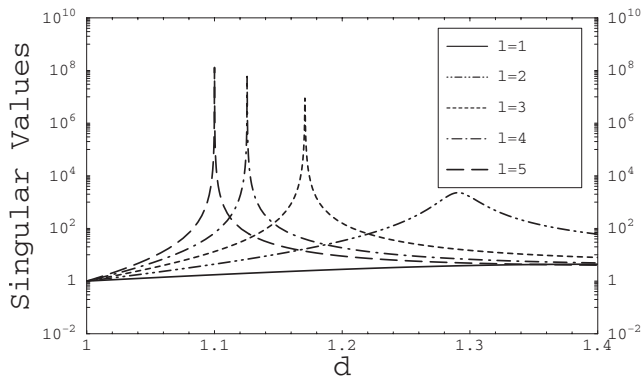


FIG. 6. Logarithmic plot of the normalized singular values $[\rho_l^{(1)}]^2$ for a $\lambda/4$ antenna versus the radii ratio $d \equiv b/a$. The inner sphere is assumed not to contain any material (i.e., $\epsilon_a=1=\mu_a$) and the surrounding shell is assumed to be a lossless DNG material with $\mu_b=-1$ and $x_b=-50 \text{ m}^{-1}$.

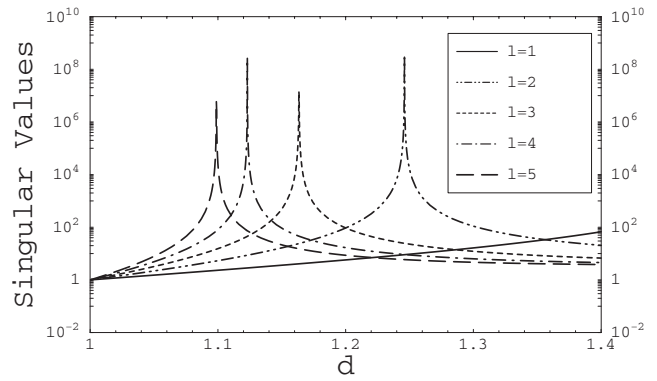


FIG. 7. Logarithmic plot of the normalized electric singular values $[\rho_l^{(1)}]^2$ for a $\lambda/40$ antenna versus the radii ratio $d \equiv b/a$. The inner sphere is assumed not to contain any material (i.e., $\epsilon_a=1=\mu_a$) and the surrounding shell is assumed to be a lossless DNG material with $\mu_b=-1$ and $x_b=-50 \text{ m}^{-1}$.

launching ability of the antenna for different modes, appear at certain fixed values of the radii ratio d . This indicates that for a small enough k_0a the enhancement for all the modes appears at certain specified values of d regardless of the total physical dimensions of the antenna. This is in total agreement with the reported subwavelength resonator concept [15,42,43] where the determining parameter for the existence of a natural mode (polariton), and thus the occurrence of a local enhancement in the launching ability of the antenna in this case, turns out to be the ratio of the two radii rather than the total physical size of the antenna itself as would be the case in the presence of only ordinary media. This clearly shows that encompassing a subwavelength antenna in a judiciously chosen DNG metamaterial shell makes it possible to distribute the resources of the antenna in a fashion that is as efficient as that made possible only through the use of a much larger volume in free space.

A natural continuation to our previous investigation of the radiation efficiency of an electrically small antenna embedded in a metamaterial substrate is displayed in Fig. 9. In this figure the normalized singular values $[\rho_l^{(1)}]^2$ for a $\lambda/400$ antenna have been plotted versus the radii ratio d . The shell

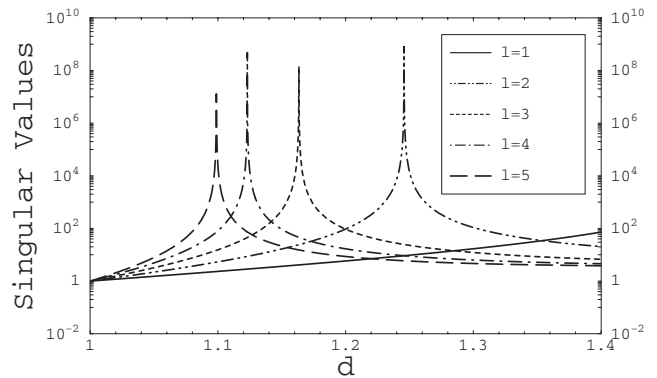


FIG. 8. Logarithmic plot of the normalized electric singular values $[\rho_l^{(1)}]^2$ for a $\lambda/400$ antenna versus the radii ratio $d \equiv b/a$. The inner sphere is assumed not to contain any material (i.e., $\epsilon_a=1=\mu_a$) and the surrounding shell is assumed to be a lossless DNG material with $\mu_b=-1$ and $x_b=-50 \text{ m}^{-1}$.

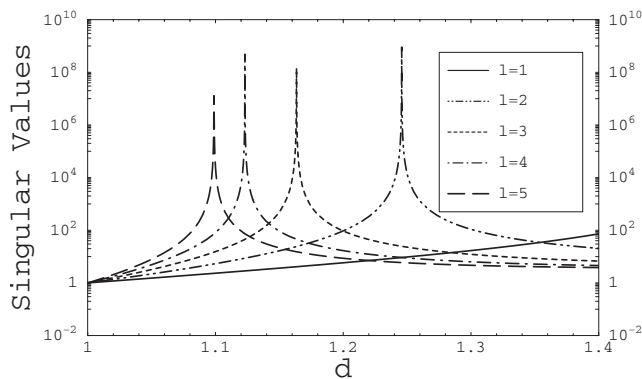


FIG. 9. Logarithmic plot of the normalized singular values $[\rho_l^{(1)}]^2$ for a $\lambda/400$ antenna versus the radii ratio $d \equiv b/a$. The inner sphere is assumed not to contain any material (i.e., $\epsilon_a = 1 = \mu_a$) and the surrounding shell is assumed to be an ENG material with $\mu_b = 1$ and $x_b = i50 \text{ m}^{-1}$.

circumscribing the antenna is assumed to be an ENG material with $\mu_b = 1$ and $x_b = i50 \text{ m}^{-1}$ (i.e., $\epsilon_b = -4$). A comparison of Figs. 9 and 8 shows that these figures are in fact the same though they describe two totally different systems. This clearly demonstrates the fact that one can attain the same level of performance achieved through the utilization of a DNG shell by using an SNG (in this case an ENG) shell. This, too, is in total agreement with the results reported in the literature [[9,15,16,42,43],] which stipulate that the use of DNG media is not really necessary in order to achieve high performance levels and that similar performance levels could be achieved by pairing two materials that possess oppositely signed values of at least one of the constitutive parameter. (In our case we had on one hand a DPS medium, i.e., the vacuum core, and on the other hand the ENG shell such that $\mu_b = 1 = \mu_a$ while $\epsilon_b = -4 = -4\epsilon_a$.) The problem of pairing other types of substrates, such as an MNG core and an ENG shell, has also been considered and the obtained results are consistent with the published literature. Attaining high performance levels, such as high radiation enhancement, through the utilization of an ENG medium is an interesting possibility since such media exist in nature (plasmonic materials such as silver, etc.).

B. Lossy substrates

The case of lossy substrates is illustrated in Fig. 10. In this figure the normalized electric singular values $[\rho_l^{(1)}]^2$ have been plotted versus the radii ratio d for a $\lambda/400$ antenna embedded in a vacuum-core-DNG-shell system. The surrounding DNG shell is assumed to have a magnetic permeability $\mu_b = -1$ and $\text{Re}[x_b] = -150 \text{ m}^{-1}$ (i.e., $\text{Re}[\epsilon_b] = -36$). The investigated cases are (1) lossless case (loss tangent $\text{Im}[\epsilon_b]/\text{Re}[\epsilon_b] = 0$), (2) DNG shell with loss tangent $\text{Im}[\epsilon_b]/\text{Re}[\epsilon_b] \approx 1/60$, and (3) DNG shell with loss tangent $\text{Im}[\epsilon_b]/\text{Re}[\epsilon_b] \approx 1/20$. Figure 10 clearly shows that the inclusion of losses simply reduces the heights of the peaks but does not make the peaks disappear. Also the decrease in the height of the resonant peaks becomes larger relative to the lossless cases as the loss tangent of the shell increases. These

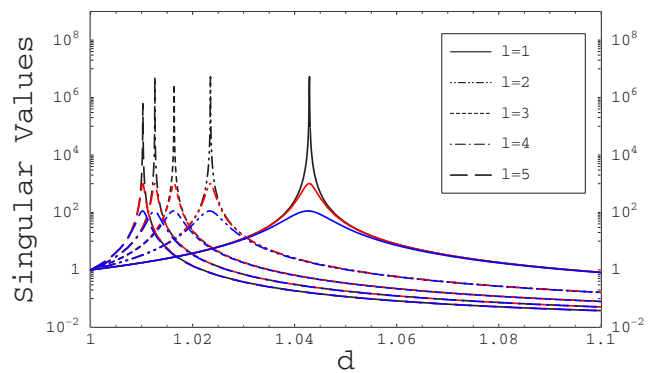


FIG. 10. (Color online) Logarithmic plot of the normalized electric singular values $[\rho_l^{(1)}]^2$ for a $\lambda/400$ antenna versus the radii ratio $d \equiv b/a$. The inner sphere is assumed not to contain any material (i.e., $\epsilon_a = 1 = \mu_a$) and the surrounding shell is assumed to be a lossless DNG material (black curves), a lossy DNG shell with a loss tangent set to $1/20$ (blue or dark gray curves), and a lossy DNG material with a loss tangent set to $1/60$ (red or light gray curves). In all three cases $\mu_b = -1$, $\text{Re}[x_b] = -150 \text{ m}^{-1}$.

findings are not surprising and are in agreement with the results reported in the literature [15,16,42,43].

1. Further look at the electric dipole case

We now initiate an investigation focused on the electric dipole case, i.e., in this case $j=1=l$. We define the electric dipole antenna gain as $G \equiv \mathcal{E}_{\text{ME}}^{(j=1=l)}(\text{free-space case}) / \mathcal{E}_{\text{ME}}^{(j=1=l)} = [\rho_1^{(1)}]^2$. This quantity is plotted next versus the radii ratio d for some representative systems and some selected values of the shell wave number x_b . The systems considered here are electric dipoles of different physical sizes embedded in vacuum-core-DNG-shell systems. As explained above this means that in all the cases the inner sphere is assumed not to contain any material, i.e., $\epsilon_a = 1 = \mu_a$, while the outer shell is made up of a DNG material with $\mu_b = -1$. The driving frequency f is still set to 3.75 GHz .

In Figs. 11–13 the gain G has been plotted versus the radii ratio d for a $\lambda/4$ -electric-dipole antenna ($a=1 \text{ cm}$), a $\lambda/40$ -electric-dipole antenna ($a=0.1 \text{ cm}$), and a $\lambda/400$ -electric-dipole antenna ($a=0.01 \text{ cm}$). The aim is to

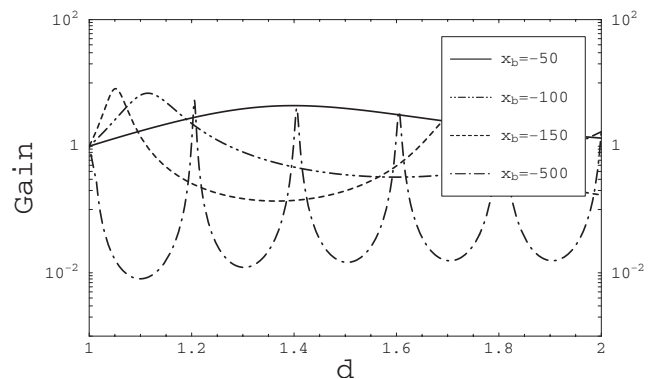


FIG. 11. Logarithmic plot of the gain G for a $\lambda/4$ -electric-dipole antenna versus the radii ratio $d \equiv b/a$. The surrounding shell is assumed to be a DNG material with $\mu_b = -1$.

study the effect of the physical size a on the performance of the antenna. From Figs. 11–13 we notice that there is something that is counterintuitive here. It appears that as the physical size of the dipole antenna becomes smaller the antenna’s ability to optimize the utilization of its resources to radiate the dipolar field efficiently increases. This is counterintuitive because what one would expect is that as the volume encompassing the antenna decreases it becomes more difficult to distribute the resources of the antenna so as to allow the antenna to radiate efficiently [33–35,71,72]. The explanation of this seemingly counterintuitive situation lies in the physical interpretation of the resonant peaks. As established above the resonant peaks correspond to the presence of polaritons. These polaritons have a certain dispersion relation, viz., Eq. (23) for the electric modes and Eq. (24) for the magnetic modes. These dispersion relations, or resonance conditions, establish a certain relationship between the different parameters relevant to the problem. When all the parameters are fixed except for the physical size of the antenna, as is the situation in this case, one should be able, at least numerically, to solve for the optimum value of the physical size that would satisfy the resonance condition. This optimal value of the physical size of the antenna is what we are dealing with in this case. However, if this is true then values on both sides of this optimal size should cause a reduction in the ability of the antenna to radiate the dipolar field which is no the case. The simulations show that as the physical size of the antenna is reduced further the resonant peaks remain at the same location. This objection may be explained away by invoking the concept of subwavelength resonator [15,42,43]. Indeed, if the optimal value of the physical size turns out to satisfy the subwavelength resonator conditions [15,42,43], that is, if the size of the core-shell system turns out to be smaller than the wavelength in all three regions then further reducing the physical size of the antenna will not affect the radiation performance of the antenna, as discussed above.

V. CONCLUSION AND FUTURE DIRECTIONS

To conclude, we have investigated, both analytically and numerically, the effects that the presence of metamaterials

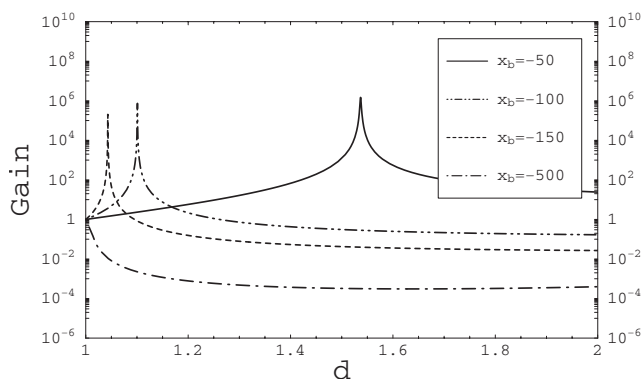


FIG. 12. Logarithmic plot of the gain G for a $\lambda/40$ -electric-dipole antenna versus the radii ratio $d \equiv b/a$. The surrounding shell is assumed to be a DNG material with $\mu_b = -1$.

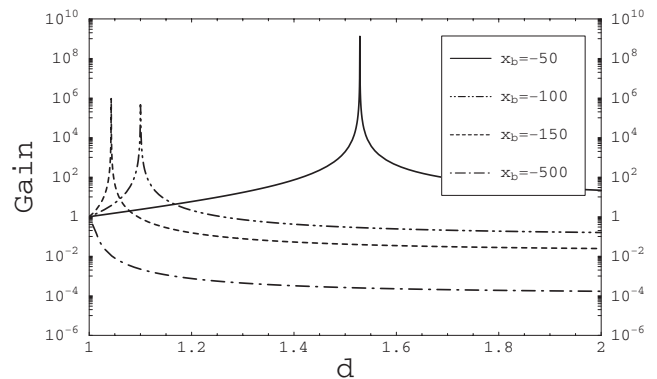


FIG. 13. Logarithmic plot of the gain G for a $\lambda/40$ -electric-dipole antenna versus the radii ratio $d \equiv b/a$. The surrounding shell is assumed to be a DNG material with $\mu_b = -1$.

would have on the performance of a general antenna embedded in a generally lossy system of two nested spheres (core-shell system) in terms of the efficiency with which the available resources of the antenna could be distributed within a prescribed volume so as to generate a given radiated field. The derived developments constitute a fundamental inverse-source-theoretic framework for analysis and design of different substrate structures. This framework also complements in analytical and computational tools and insight the pioneering work by some of the leading authors in this area.

The adoption of the inverse-source-theoretic approach is aimed at enabling intrinsic, i.e., non-antenna-specific, and fair characterization of different substrate configurations by comparing optimal radiation in either configuration (i.e., the “best” in each one). This characterization is governed by a formally tractable source-energy cost function that is physically motivated by Ohmic loss control. Via analytical and numerical examples we have explained and illustrated important enhancements due to the presence of metamaterials in the context of the two-nested-spheres configuration, in particular for media with oppositely signed constitutive parameters.

Our study also relates to the inverse scattering investigations that constitute a subject of interest of our group. In particular, in this other motivational context, the goal is to enhance imaging resolution of an object under active interrogation thanks to multiple scattering interactions of the object with a helper substrate that acts as a near-field agent (a “retransmitting station”) that facilitates communication to the far field of evanescent field information about the object. In fact, the achieving of super-resolution thanks to multiple scattering, and the reevaluation of the so-called “diffraction limit” in imaging, is an area that has been receiving much attention in recent years, and is closely connected to the developments in radiation and scattering enhancement due to metamaterials. As in the metamaterial field, subwavelength resonances in rather simple multiple scattering systems (including systems of only two closely spaced small scatterers) have also been of interest [73–76]. A natural future direction for continuation of the research reported in this work is to expand our analysis to the full inverse scattering problem in metamaterial substrates including multiple scattering, as well

as to quantitatively characterize the “enhancement” in imaging in the presence of noise via the fundamental Cramer-Rao bound along the lines considered in Refs. [75,76] and in the references therein. As suggested in Ref. [77], where super-resolution “intensity-only” (phaseless information) imaging is investigated, the use of metamaterials can also play a major role in optical imaging with phaseless data, particularly in the imaging with far field data (by acting as “station” capturing evanescent field information), and this is another interesting open area for further exploration. We plan to address these and related matters elsewhere.

ACKNOWLEDGMENTS

This work was supported by the United States Air Force Office of Scientific Research under Grant No. FA9550-06-01-0013 and by the National Science Foundation under Grant No. 0746310.

APPENDIX: WAVE FUNCTIONS $\mathfrak{B}_{l,m}^{(j)}$ FOR A SYSTEM OF TWO NESTED SPHERES

The aim of this appendix is to show that the multipole moments $a_{l,m}^{(j)}$ are given by Eq. (10) with the source-free wave functions $\mathfrak{B}_{l,m}^{(j)}(\mathbf{r})$ given by Eqs. (11) and (12). A straightforward way of arriving at these results would be to use the dyadic Green’s function that governs the propagation of electromagnetic radiation between the source-enclosing inner sphere and the surrounding vacuum in the three-region geometry under investigation. The spectral-domain electromagnetic Green’s function linking the different layers of a spherically multilayered medium has been calculated by Li *et al.* [78]. [For the three-region geometry under consideration the Green function is given in Ref. [78] by Eqs. (14),(29a)–(29d), and the relevant definitions.] Afterwards one calculates the electric field outside V by means of Eq. (2) (in Ref. [78]). Finally one uses Eqs. (8) and (9), in this paper, to arrive at the desired results, i.e., Eqs. (10)–(12).

Another way of arriving at Eqs. (10)–(12) is to invoke Lorentz’s reciprocity theorem and the concept of reaction (also called coupling). Here we adopt this approach. One reason behind this choice is that this latter approach attests to the visible similarity between the mathematics of the radiation problem at hand and its scattering counterpart (investigated in Ref. [41] for conventional materials and in Ref. [42] for metamaterials.) The reaction of a field $\mathbf{E}(\mathbf{r})$ produced by a source $\mathbf{J}(\mathbf{r})$ on another source $\mathbf{J}_0(\mathbf{r})$, is defined as $\int d\mathbf{r} \cdot \mathbf{E}(\mathbf{r}) \cdot \mathbf{J}_0(\mathbf{r}) \equiv \mathcal{R}_{\mathbf{E} \rightarrow \mathbf{J}_0}$. The reciprocity theorem can be stated as follows (see, for instance, Ref. [62]): the reaction of the field $\mathbf{E}(\mathbf{r})$ produced by a source $\mathbf{J}(\mathbf{r})$ on another source

$\mathbf{J}_0(\mathbf{r})$ is equal to the reaction of the field $\mathbf{E}_0(\mathbf{r})$ produced by the source $\mathbf{J}_0(\mathbf{r})$ on the source $\mathbf{J}(\mathbf{r})$, i.e., $\mathcal{R}_{\mathbf{E} \rightarrow \mathbf{J}_0} = \mathcal{R}_{\mathbf{E}_0 \rightarrow \mathbf{J}}$ or, explicitly,

$$\int d\mathbf{r} \cdot \mathbf{E}(\mathbf{r}) \cdot \mathbf{J}_0(\mathbf{r}) = \int d\mathbf{r} \cdot \mathbf{E}_0(\mathbf{r}) \cdot \mathbf{J}(\mathbf{r}). \quad (\text{A1})$$

To evaluate the field due to a current distribution $\mathbf{J}(\mathbf{r})$ that is embedded in the piecewise-constant background of interest, we conveniently consider, without loss of generality, the following two classes of canonical sources:

$$[\mathbf{J}_{l,m}^{(1)}]_0(\mathbf{r}) = \delta(r-R)\hat{\mathbf{r}} \times \mathbf{Y}_{l,m}(\hat{\mathbf{r}}) \quad (\text{A2})$$

and

$$[\mathbf{J}_{l,m}^{(2)}]_0(\mathbf{r}) = \delta(r-R)\mathbf{Y}_{l,m}(\hat{\mathbf{r}}), \quad (\text{A3})$$

where in both expressions $R > b$ represents the radius of the helper source centered around the origin. Ultimately, our calculation of the multipole moments $a_{l,m}^{(j)}$ will be independent of R . The justification for the calculation methodology based on these helper sources will become evident next, but here we wish to mention two key facts: (1) the transverse component of an arbitrary vector field on the spherical surface of radius $R > b$ centered about the origin is uniquely characterized by its expansion in terms of the vector spherical harmonics $\mathbf{Y}_{l,m}(\hat{\mathbf{r}})$ and their associated vector functions $\hat{\mathbf{r}} \times \mathbf{Y}_{l,m}(\hat{\mathbf{r}})$ [63] and (2) the multipole moments characterizing any electric field outside the support of the emitting source are uniquely determined by the tangential component of the field on any such spherical surface. Indeed, it can easily be shown that if $R > b$ is the radius of a sphere centered about the origin, then

$$a_{l,m}^{(j)} = \begin{cases} \frac{-i}{l(l+1)k_0 h_l^{(+)}(k_0 R)} \int \mathbf{Y}_{l,m}^*(\hat{\mathbf{r}}) \cdot \mathbf{E}(R\hat{\mathbf{r}}) d\hat{\mathbf{r}}, & j=1, \\ \frac{1}{l(l+1)k_0 V_l(k_0 R)} \int \hat{\mathbf{r}} \times \mathbf{Y}_{l,m}^*(\hat{\mathbf{r}}) \cdot \mathbf{E}(R\hat{\mathbf{r}}) d\hat{\mathbf{r}}, & j=2. \end{cases} \quad (\text{A4})$$

The field $[\mathbf{E}_{l,m}^{(j)}]_{inc}$ that would be produced in the vacuum by the source $[\mathbf{J}_{l,m}^{(j)}]_0$ [defined in Eq. (A3)] is given by

$$[\mathbf{E}_{l,m}^{(j)}]_{inc} = \int d\mathbf{r}' \bar{\mathbf{G}}_0(\mathbf{r}, \mathbf{r}') \cdot [\mathbf{J}_{l,m}^{(j)}]_0(\mathbf{r}'), \quad (\text{A5})$$

where $\bar{\mathbf{G}}_0(\mathbf{r}, \mathbf{r}')$ is the multipole representation of the free-space electric dyadic Green function, viz. [79],

$$\begin{aligned} \bar{\mathbf{G}}_0(\mathbf{r}, \mathbf{r}') = & \sum_{l=1}^{\infty} \sum_{m=-l}^l \frac{-\omega\mu_0}{k_0 l(l+1)} \{ k_0^2 [j_l(k_0 r_{<}) \mathbf{Y}_{l,m}(\hat{\mathbf{r}}_{<})] [h_l^{(+)}(k_0 r_{>}) \mathbf{Y}_{l,m}^*(\hat{\mathbf{r}}_{>})] \\ & + \nabla \times [j_l(k_0 r_{<}) \mathbf{Y}_{l,m}(\hat{\mathbf{r}}_{<})] \nabla \times [h_l^{(+)}(k_0 r_{>}) \mathbf{Y}_{l,m}^*(\hat{\mathbf{r}}_{>})] \} + \frac{i}{\omega\epsilon_0} \hat{\mathbf{r}} \delta(\mathbf{r} - \mathbf{r}'). \end{aligned} \quad (\text{A6})$$

The $\langle \rangle$ subscript designates the smaller (larger) of r and r' . This field $[\mathbf{E}_{l,m}^{(j)}]_{\text{inc}}$ will be referred to as the incident field in the following.

For $r < R$ the incident field $[\mathbf{E}_{l,m}^{(2)}]_{\text{inc}}$ is found to be given by

$$[\mathbf{E}_{l,m}^{(2)}]_{\text{inc}}(\mathbf{r}) = \zeta_l(k_0 R) j_l(k_0 r) \mathbf{Y}_{l,m}(\hat{\mathbf{r}}), \quad (\text{A7})$$

where we have introduced $\zeta_l(k_0 R) \equiv -(k_0 R)^2 \eta_0 h_l^{(+)}(k_0 R)$. Along analogous lines, the incident field $[\mathbf{E}_{l,m}^{(1)}]_{\text{inc}}$ produced

by the source $[\mathbf{J}_{l,m}^{(1)}]_0$ in Eq. (A2) in free space is found, using the same route, to be given for $r < R$ by

$$[\mathbf{E}_{l,m}^{(1)}]_{\text{inc}}(\mathbf{r}) = \tau_l(k_0, R) \nabla \times [j_l(k_0 r) \mathbf{Y}_{l,m}(\hat{\mathbf{r}})], \quad (\text{A8})$$

where we have defined $\tau_l(k_0, R) \equiv -\eta_0 k_0 R^2 V_l(k_0 R)$. The obtaintment of the above results requires the use of orthogonality properties of the vector spherical harmonics $\mathbf{Y}_{l,m}(\hat{\mathbf{r}})$ and the associated vector functions $\hat{\mathbf{r}} \times \mathbf{Y}_{l,m}(\hat{\mathbf{r}})$.

The total field $[\mathbf{E}_{l,m}^{(1)}]_0$ must be, due to considerations of causality in the scattered field and well-behavedness of the interior field for $r < b$, of the form

$$[\mathbf{E}_{l,m}^{(1)}]_0(\mathbf{r}) = \begin{cases} \nabla \times [\tau_l(k_0, R) j_l(k_0 r) \mathbf{Y}_{l,m}(\hat{\mathbf{r}}) + D_1 h_l^{(+)}(k_0 r) \mathbf{Y}_{l,m}(\hat{\mathbf{r}})], & r > b, \\ \nabla \times [B_1 j_l(k_b r) \mathbf{Y}_{l,m}(\hat{\mathbf{r}}) + C_1 h_l^{(+)}(k_b r) \mathbf{Y}_{l,m}(\hat{\mathbf{r}})], & a < r \leq b, \\ A_1 \nabla \times [j_l(k_a r) \mathbf{Y}_{l,m}(\hat{\mathbf{r}})], & r \leq a, \end{cases} \quad (\text{A9})$$

where A_1, B_1, C_1 , and D_1 are coefficients that are to be determined by imposing continuity of the tangential components of the electric and magnetic fields on the inner and outer boundaries of the spherical shell. Analogously, the total field $[\mathbf{E}_{l,m}^{(2)}]_0$ must be of the form

$$[\mathbf{E}_{l,m}^{(2)}]_0(\mathbf{r}) = \begin{cases} [\zeta_l(k_0 R) j_l(k_0 r) + D_2 h_l^{(+)}(k_0 r)] \mathbf{Y}_{l,m}(\hat{\mathbf{r}}), & r > b, \\ [B_2 j_l(k_b r) + C_2 h_l^{(+)}(k_b r)] \mathbf{Y}_{l,m}(\hat{\mathbf{r}}), & a < r \leq b, \\ A_2 j_l(k_a r) \mathbf{Y}_{l,m}(\hat{\mathbf{r}}), & r \leq a, \end{cases} \quad (\text{A10})$$

where A_2, B_2, C_2 , and D_2 are coefficients that need to be determined from the boundary conditions.

Imposing the abovementioned continuity requirements on the inner and outer boundaries of the spherical shell, i.e., on the spheres of radii a and b , respectively, yields two systems (one for $j=1$ and one for $j=2$) of four equations each linear in the unknown coefficients. Upon solving the two linear systems of equations and using the Wronskian relation for spherical Bessel functions, specifically $j_l(x) h_l'^{(+)}(x) - j_l'(x) h_l^{(+)}(x) = \frac{i}{x^2}$ [64], we find that for $j=1$

$$\frac{A_1}{\tau_l(k_0, R)} = \frac{\epsilon_b}{\Delta_1 k_0 k_b a^2 b^2} \equiv \mathfrak{F}_l^{(1)}, \quad (\text{A11})$$

where Δ_1 is the determinant given by Eq. (13). Similarly for $j=2$ one obtains

$$\frac{A_2}{\zeta_l(k_0 R)} = \frac{1}{\mu_b \Delta_2 k_0 k_b a^2 b^2} \equiv \mathfrak{F}_l^{(2)}, \quad (\text{A12})$$

where Δ_2 is the determinant given by Eq. (14). The remaining constants B_1, C_1, D_1, B_2, C_2 , and D_2 are straightforwardly obtained; here they are omitted because of their irrelevance to the rest of the problem. Along with Eqs. (A9) and (A10), Eqs. (A11) and (A12) define the fields $[\mathbf{E}_{l,m}^{(2)}]_0$ and $[\mathbf{E}_{l,m}^{(1)}]_0$ in the region V .

By applying the reciprocity theorem Eq. (A1) to the preceding results [in particular, Eqs. (A2), (A3), and (A9)–(A12)], one finds that the multipole moments $a_{l,m}^{(j)}$ are indeed

independent of R and given by Eq. (10) with the source-free wave functions $\mathfrak{B}_{l,m}^{(j)}$ given by Eqs. (11) and (12) where we have also recalled the multipole expansion for the electric field $\mathbf{E}(\mathbf{r})$ (8) and (9) along with the orthogonality and analytic continuation properties of the vector spherical harmonics and the analytic continuation property of the spherical Bessel functions of the first kind, namely, $j_l^*(ka) = j_l(k^*a)$.

An alternative way of arriving at Eq. (10) and Eqs. (11) and (12) would be to use the far-field expressions instead of the multipole expansion (8) and (9). The far-field approximations for the electric and magnetic fields are expressed as [71]

$$\mathbf{E}(r\hat{\mathbf{r}}) \underset{k_0 r \gg 1}{\sim} \frac{e^{ik_0 r}}{r} \mathbf{f}_e(\hat{\mathbf{r}}) = \eta_0 \left(\frac{e^{ik_0 r}}{r} \right) \hat{\mathbf{r}} \times \mathbf{f}_m(\hat{\mathbf{r}}), \quad (\text{A13})$$

$$\mathbf{H}(r\hat{\mathbf{r}}) \underset{k_0 r \gg 1}{\sim} \left(\frac{e^{ik_0 r}}{\eta_0 r} \right) \hat{\mathbf{r}} \times \mathbf{f}_e(\hat{\mathbf{r}}) = \frac{e^{ik_0 r}}{r} \mathbf{f}_m(\hat{\mathbf{r}}), \quad (\text{A14})$$

where $\eta_0 = \sqrt{\mu_0 / \epsilon_0}$ is the free-space wave impedance. The two vector quantities $\mathbf{f}_e(\hat{\mathbf{r}})$ and $\mathbf{f}_m(\hat{\mathbf{r}})$ are, respectively, the far electric field radiation pattern and the far magnetic field radiation pattern. They are given as a function of the observation direction $\hat{\mathbf{r}}$ by

$$\mathbf{f}_e(\hat{\mathbf{r}}) = \sum_{l=1}^{\infty} \sum_{m=-l}^l (-i)^l [a_{l,m}^{(1)} \hat{\mathbf{r}} \times \mathbf{Y}_{l,m}(\hat{\mathbf{r}}) + a_{l,m}^{(2)} \mathbf{Y}_{l,m}(\hat{\mathbf{r}})] \quad (\text{A15})$$

and

$$\mathbf{f}_m(\hat{\mathbf{r}}) = \frac{1}{\eta_0} \sum_{l=1}^{\infty} \sum_{m=-l}^l (-i)^l [-a_{l,m}^{(1)} \mathbf{Y}_{l,m}(\hat{\mathbf{r}}) + a_{l,m}^{(2)} \hat{\mathbf{r}} \times \mathbf{Y}_{l,m}(\hat{\mathbf{r}})]. \quad (\text{A16})$$

It follows from Eqs. (A15) and (A16) and the orthogonality of the vector spherical harmonics $\mathbf{Y}_{l,m}(\hat{\mathbf{r}})$ and the associated vector functions $\hat{\mathbf{r}} \times \mathbf{Y}_{l,m}(\hat{\mathbf{r}})$ that the multipole moments $a_{l,m}^{(j)}$ are uniquely defined by projections of the far-field radiation patterns onto the orthogonal set of functions $\mathbf{Y}_{l,m}(\hat{\mathbf{r}})$ and $\hat{\mathbf{r}} \times \mathbf{Y}_{l,m}(\hat{\mathbf{r}})$ [see, e.g., Ref. [71], Eq. (7) and the associated

discussion]. Thus either the far fields or the multipole moments uniquely define each other as well as the exterior field everywhere outside the source volume V [via Eq. (8)].

In order to arrive at Eq. (10) and Eqs. (11) and (12) we follow the same procedure as above but instead of the multipole expansion (8) and (9) we use Eqs. (A14)–(A16). We then require that $k_0 R \gg 1$ and use the large-argument approximation for the spherical Hankel function, in particular, $h_l^{(+)}(k_0 R) \sim (-i)^{l+1} e^{ik_0 R} / (k_0 R)$ (see, for instance, Ref. [64]). Afterwards one lets $k_0 R \rightarrow \infty$. Whether one uses this approach or the previous one, the final results are the same.

-
- [1] R. W. Ziolkowski and N. Engheta, in *Metamaterials: Physics and Engineering Explorations*, edited by R. W. Ziolkowski and N. Engheta (IEEE Press/Wiley, New York, 2006), Chap. 1, pp. 5–41.
- [2] V. G. Veselago and E. E. Narimanov, *Nat. Mater.* **5**, 759 (2006).
- [3] M. Lapine and S. Tretyakov, *IET Proc. Microwaves, Antennas Propag.* **1**, 3 (2007).
- [4] D. R. Smith, W. J. Padilla, D. C. Vier, S. C. Nemat-Nasser, and S. Schultz, *Phys. Rev. Lett.* **84**, 4184 (2000).
- [5] M. Th evenot, C. Cheype, A. Reineix, and B. Jecko, *IEEE Trans. Microwave Theory Tech.* **47**, 2115 (1999).
- [6] B. Temelkuran, M. Bayindir, E. Ozbay, R. Biswas, M. M. Sigalas, G. Tuttle, and K. M. Ho, *J. Appl. Phys.* **87**, 603 (2000).
- [7] S. Enoch, G. Tayeb, P. Sabouroux, N. Gu erin, and P. Vincent, *Phys. Rev. Lett.* **89**, 213902 (2002).
- [8] A. Al u and N. Engheta, *Microw. Opt. Technol. Lett.* **35**, 460 (2002).
- [9] R. W. Ziolkowski and A. D. Kipple, *IEEE Trans. Antennas Propag.* **51**, 2626 (2003).
- [10] D. Tonn and R. Bansal, in *IEEE International Antennas and Propagation Symposium* (2005), Vol. 2A, pp. 602–605.
- [11] A. Erentok, P. L. Luljak, and R. W. Ziolkowski, *IEEE Trans. Antennas Propag.* **53**, 160 (2005).
- [12] G. Lovat, P. P. Burghignoli, F. Capolino, D. R. Jackson, and D. R. Wilton, *IEEE Trans. Antennas Propag.* **54**, 1017 (2006).
- [13] B.-I. Wu, W. Wang, J. Pacheco, X. Chen, T. Grzegorzczuk, and J. Kong, *Prog. Electromagn. Res.* **51**, 295 (2005).
- [14] S. F. Mahmoud, *IEEE Antennas Wireless Propag. Lett.* **3**, 19 (2004).
- [15] R. W. Ziolkowski and A. D. Kipple, *Phys. Rev. E* **72**, 036602 (2005).
- [16] R. W. Ziolkowski and A. Erentok, *IEEE Trans. Antennas Propag.* **54**, 2113 (2006).
- [17] S. Tretyakov, S. Maslovski, A. Sochava, and C. Simovski, *IEEE Trans. Antennas Propag.* **53**, 965 (2005).
- [18] S. A. Tretyakov and M. Ermutlu, *IEEE Antennas Wireless Propag. Lett.* **4**, 266 (2005).
- [19] A. D. Yaghjian and S. R. Best, *IEEE Trans. Antennas Propag.* **53**, 1298 (2005).
- [20] P. M. T. Ikonen, K. N. Rozanov, A. V. Osipov, P. Alitalo, and S. A. Tretyakov, *IEEE Trans. Antennas Propag.* **54**, 3391 (2006).
- [21] R. W. Ziolkowski and A. Erentok, *IET Proc. Microwaves, Antennas Propag.* **1**, 116 (2007).
- [22] A. Erentok and R. W. Ziolkowski, *IEEE Trans. Antennas Propag.* **55**, 731 (2007).
- [23] R. C. Hansen and M. Burke, *Microw. Opt. Technol. Lett.* **26**, 75 (2000).
- [24] K. Buell, H. Mosallaei, and K. Sarabandi, *IEEE Trans. Microwave Theory Tech.* **54**, 135 (2006).
- [25] H. Mosallaei and K. Sarabandi, *IEEE Trans. Antennas Propag.* **52**, 1558 (2004).
- [26] Y. Mano and S. Bae, *Proceedings of the IEEE International Symposium on Microwave Antenna Propagation and EMC Technology for the Wireless Community* (2005), Vol. 1, p. 63.
- [27] A. Al u, F. Bilotti, and N. Engheta, *IEEE Trans. Antennas Propag.* **55**, 13 (2007).
- [28] H. Mosallaei and K. Sarabandi, *IEEE Trans. Antennas Propag.* **55**, 45 (2007).
- [29] P. Ikonen, P. Alitalo, and S. Tretyakov, *Antennas Wireless Propag. Lett.* **6**, 186 (2007).
- [30] M. Hirvonen, J. C.-E. Sten, and P. K. Koivisto (private communication).
- [31] E. Rodes, L. Moustapha, L. Mercier, M. Th evenot, T. Mondeniere, and B. Jecko, in *Antennas and Propagation Conference, 2007. LAPC 2007*, Loughborough, UK (2007).
- [32] N. Engheta, A. Al u, R. W. Ziolkowski, and A. Erentok, in *Metamaterials: Physics and Engineering Explorations*, edited by N. Engheta and R. W. Ziolkowski (IEEE Press/Wiley, New York, 2006), Chap. 2, pp. 43–85.
- [33] A. J. Devaney, E. A. Marengo, and M. Li, *SIAM J. Appl. Math.* **67**, 1353 (2007).
- [34] E. A. Marengo and M. R. Khodja, *Source Synthesis in Substrate Media: Fundamental Bounds, International Symposium on Electromagnetic Theory*, URSI Commission B, Ottawa (2007).
- [35] E. A. Marengo, M. R. Khodja, and A. Boucherif (unpublished).
- [36] H. B. Keller and J. B. Keller, *J. Appl. Phys.* **20**, 393 (1949).
- [37] M. G. Andreasen, *IRE Trans. Antennas Propag.* **5**, 337 (1957).
- [38] R. V. Row, *IEEE Trans. Antennas Propag.* **12**, 646 (1964).
- [39] D. E. Burrick, in *Radar Cross Section Handbook*, edited by G. T. Ruck, D. E. Burrick, W. D. Stuart, and C. K. Krichbaum (Plenum Press, New York, 1970), Vol. 1, Chap. 3.
- [40] L. Gao and Y. Huang, *Opt. Commun.* **239**, 25 (2004).
- [41] A. L. Aden and M. Kerker, *J. Appl. Phys.* **22**, 1242 (1951).

- [42] A. Alù and N. Engheta, *J. Appl. Phys.* **97**, 094310 (2005).
- [43] A. Alù and N. Engheta, *J. Appl. Phys.* **99**, 069901 (2006).
- [44] R. W. Ziolkowski and E. Heyman, *Phys. Rev. E* **64**, 056625 (2001).
- [45] A. J. Devaney and E. Wolf, *Phys. Rev. D* **8**, 1044 (1973).
- [46] E. A. Marengo and M. R. Khodja, *Phys. Rev. E* **74**, 036611 (2006).
- [47] G. Kaiser, *J. Phys. A* **38**, 495 (2005).
- [48] A. J. Devaney, G. Kaiser, E. A. Marengo, R. Albanese, and G. Erdmann, *IEEE Trans. Antennas Propag.* (to be published).
- [49] R. P. Porter and A. J. Devaney, *J. Opt. Soc. Am.* **72**, 327 (1982).
- [50] R. P. Porter and A. J. Devaney, *J. Opt. Soc. Am.* **72**, 1707 (1982).
- [51] K. J. Langenberg, in *Basic Methods of Tomography and Inverse Problems*, edited by P. C. Sabatier (Adam Hilger, Bristol, 1987), pp. 128–467.
- [52] T. S. Angell, A. Kirsch, and R. E. Kleinman, *Proc. IEEE* **79**, 1559 (1991).
- [53] O. M. Bucci, G. D’Elia, G. Mazzarella, and G. Panariello, *Proc. IEEE* **82**, 358 (1994).
- [54] D. Liu, R. J. Garbacz, and D. M. Pozar, *IEEE Trans. Antennas Propag.* **38**, 862 (1990).
- [55] Y. T. Lo, S. W. Lee, and Q. W. Lee, *Proc. IEEE* **54**, 1033 (1966).
- [56] G. A. Deschamps and H. S. Cabayan, *IEEE Trans. Antennas Propag.* **20**, 268 (1972).
- [57] F. Cakoni and D. Colton, *Qualitative Methods in Inverse Scattering Theory* (Springer, Berlin, 2006).
- [58] R. Potthast, *Point Sources and Multipoles in Inverse Scattering Theory* (Chapman and Hall/CRC, Boca Raton, Florida, 2001).
- [59] E. A. Marengo, F. K. Gruber, and F. Simonetti, *IEEE Trans. Image Process.* **16**, 1967 (2007).
- [60] J. A. Stratton, *Electromagnetic Theory* (McGraw Hill, New York, 1941).
- [61] J. D. Jackson, *Classical Electrodynamics* (Wiley, New York, 1999).
- [62] C. A. Balanis, *Advanced Engineering Electromagnetics* (Wiley, New York, 1989).
- [63] A. J. Devaney and E. Wolf, *J. Math. Phys.* **15**, 234 (1974).
- [64] G. B. Arfken and H. J. Weber, *Mathematical Methods for Physicists* (Academic Press, New York, 2005).
- [65] R. F. Harrington, *IRE Trans. Antennas Propag.* **6**, 219 (1958).
- [66] R. E. Collin, *Field Theory of Guided Waves* (IEEE Press, New York, 1991).
- [67] E. A. Marengo, A. J. Devaney, and F. K. Gruber, *IEEE Trans. Antennas Propag.* **52**, 1586 (2004).
- [68] M. R. Khodja and E. A. Marengo (unpublished).
- [69] S. R. Best, *IEEE Antennas Propag. Mag.* **46**, 9 (2004).
- [70] M. Abramowitz and I. A. Stegun, *Handbook of Mathematical Functions* (Dover, New York, 1964).
- [71] E. A. Marengo and A. J. Devaney, *IEEE Trans. Antennas Propag.* **47**, 410 (1999).
- [72] E. A. Marengo and R. W. Ziolkowski, *IEEE Trans. Antennas Propag.* **48**, 1553 (2000).
- [73] F. Simonetti, *Phys. Rev. E* **73**, 036619 (2006).
- [74] F. Simonetti, *Phys. Rev. E* **75**, 048602 (2007).
- [75] F. Simonetti, M. Fleming, and E. A. Marengo, *J. Opt. Soc. Am. A* **25**, 292 (2008).
- [76] E. A. Marengo and F. K. Gruber, *EURASIP J. Appl. Signal Process.* **2007**, 17342 (2007).
- [77] E. A. Marengo, R. D. Hernandez, and H. Lev-Ari, *J. Opt. Soc. Am. A* **24**, 3619 (2007).
- [78] L.-W. Li, P.-S. Kooi, M.-S. Leong, and T.-S. Yeo, *IEEE Trans. Microwave Theory Tech.* **42**, 2302 (1994).
- [79] C. T. Tai, *Dyadic Green’s Functions in Electromagnetic Theory* (Intext Educational, Scranton, PA, 1971).